18th Australasian Fluid Mechanics Conference
Launceston, Australia
3-7 December 2012

Effect of chordwise flexure profile on aerodynamic performance of a flexible flapping airfoil

S. Premachandran and M. Giacobello

Air Vehicles Division
Defence Science and Technology Organization, Australia

Abstract

Two-dimensional Computational Fluid Dynamics (CFD) is used to assess the aerodynamic performance of various chordwise flexure profiles for an airfoil undergoing sinusoidal heaving with an oncoming free stream velocity. The aerodynamic power requirements are found to be relatively insensitive to flexure profile, while thrust generation is significantly affected and dependent primarily on the area 'swept' by the deflected chord line.

Introduction

Recent interest in the development of micro-air-vehicles (MAVs) has led engineers and scientists to take inspiration from the flapping-wing flight of insects and birds. In these low-Reynolds-number regimes, flapping-wing flyers can operate with greater efficiency and manoeuvrability than a conventional aircraft. Their relatively thin wings experience high cyclic inertial and aerodynamic loading, which leads to a significant degree of flexure which cannot be ignored in predicting performance. From a MAV design perspective, it is important to ascertain the effect of wing deformation profile on the aerodynamic performance, with a view towards designing a wing structure that can deform with improved aerodynamics characteristics.

Several previous studies (e.g. [4],[5],[8]) have indicated that, in addition to minimizing the weight penalty, the flexure of thin insect wings can actually contribute to aerodynamic performance. Insect wings may experience both spanwise and chordwise flexure; for the purpose of building an understanding of the aerodynamic contributions, this study is constrained to chordwise flexibility.

Previous experimental [4] and numerical [1],[8] studies have found that chordwise flexure can increase thrust production and decrease power consumption of a sinusoidally flapping wing. Experimental studies [4],[10] have investigated the effect of flexibility by testing wings with varying stiffness. Tang [8] used coupled 2-D fluid-structure interaction (FSI) simulations to predict the performance characteristics of wings with varying thicknesses, and found that increasing the airfoil flexibility increased thrust and decreased lift. These studies suggested that a moderate level of chordwise flexibility may improve aerodynamic performance. However, from an MAV-design perspective, it is useful to identify whether any particular form of the chordwise flexibility offers aerodynamic advantages. Miao & Ho [7] performed 2D CFD simulations on a heaving airfoil with quadratic chordwise flexure, where the leading edge underwent simple heaving and the wing chord deformation took a quadratic profile from leading edge to trailing edge. A number of parameters were investigated, including the effect of the phasing between heaving (flapping) and flexure, and the effect of the tip-deflection magnitude. The current study uses this work as a validation case, and then extends the study to other forms of flexure.

Problem description

Airfoil motion and flexure

The free stream conditions and the flapping/flexing frequency are set to replicate the parameters used by Miao & Ho [7]. The Reynolds number, based on wing chord, c, and free stream velocity, V_∞, *is* $Re = 10^4$, while the reduced frequency is $k = \omega c / V_\infty = 2$, where ω is the wing flapping frequency.

The flapping motion is prescribed as a sinusoidal heaving of the airfoil section, governed by

$$y_{heaving} = h_0 \sin(\omega t). \quad (1)$$

The wing 'flexing' motion is superimposed on the heaving motion and is also sinusoidal but varies along the chordwise position (x) of the wing and is governed by

$$y_{flexing} = a_0 \cdot f(x) \cdot \sin(\omega t + \psi). \quad (2)$$

The wing deformation is assumed to occur only in the vertical (y) direction. For relatively low values of tip flexure this assumption is reasonable and the approach that has been used in other studies including Tang [8]. The phase lag, ψ, is set to $-\pi/2$, following the work of [7] who found this value to yield the highest propulsive efficiency. The function *f(x)* varies from zero at the airfoil leading edge ($x = 0$) to 1 at the trailing edge ($x = 1$), so that the maximum trailing edge deflection is a_0, where in most cases a_0 is set to 0.2. The different forms of *f(x)* tested in this study are given in Table 1 and cover multiple leading-edge gradients and local deflection amplitudes, as shown in Figure 1.

Description	*f(x)*
Linear	x
Quadratic	x^2
Cubic	x^3
Quadratic-2	$0.5x + 0.5x^2$

Table 1. Table of basic flexing profiles used in this study.

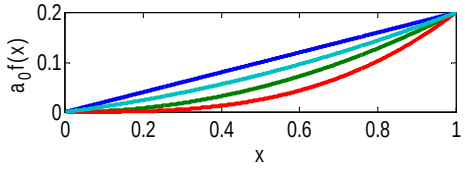

Figure 1. Illustration of flexure profiles in Table 1, with $a_0 = 0.2$:
cubic; quadratic; quadratic-2; linear.

Output Parameters

For a flapping wing in forward flight, the performance parameters of interest are thrust, input power, and efficiency. The free stream velocity is in the x direction, so the thrust, T, is defined as the force in the -x direction and the thrust power, P, is calculated as TV_∞. The input power is calculated on the vertical (y-direction) heaving and flexing motion, and so is calculated from the lift force, L, and the local y-velocity of the wing v_y according to

$$P = \int_{wing} v_y \cdot dL \ . \tag{3}$$

The forces and power are non-dimensionalised to a thrust coefficient C_T and a power coefficient C_p using V_∞ as the reference velocity and c as the reference area. The efficiency is quantified as the cycle-averaged thrust power normalised by the cycle-averaged input power,

$$\eta = \overline{C_T} V_\infty \big/ \overline{C_P} \, . \tag{4}$$

Numerical Methodology

Airfoil and Domain Geometry

The majority of the study uses an airfoil with a NACA0005 section, selected because thin wing airfoil sections are more common in insects and birds and have been shown to perform slightly better than thicker airfoils [1],[6]. However the flow over a NACA0014 section is computed to validate the present study against Miao & Ho [7].

The computational domain consists of the airfoil at the centre of a circular boundary of diameter 60c. At this distance boundary-interference effects are expected to be negligible. For the purpose of imposing the wing deflection motion, the domain is subdivided into two regions. The inner region (shown in Figure 2) extends two chord lengths from the airfoil and deforms with the airfoil**.** This is described in more detail in the following section.

Kinematics and Remeshing

The net motion of the wing is a superposition of two components: heaving and flexing. The heaving is simulated by the addition of a source term in the y-momentum equation across the whole domain, and the addition of a vertical velocity component at the far-field boundary given by $V_y = -\dot{y}_{heaving}$. The flexing motion is imposed only over the inner mesh region and airfoil. Upstream of the wing there is no mesh deformation, while across the length of the wing, the entire mesh of the inner region moves according to y_{flexing} as specified in Eq. (2). Downstream of the trailing edge, the mesh moves with the trailing-edge velocity, to ensure that a quality conformal mesh is maintained in the near wake.

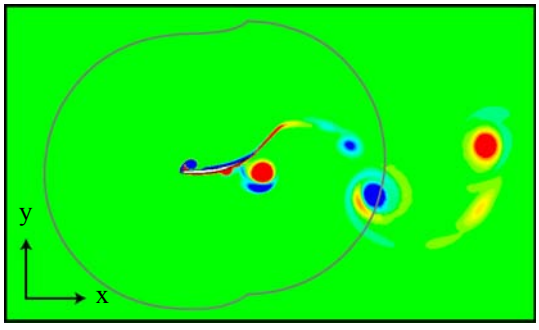

Figure 2. Example of maximum deflection for cubic flexure case: contours of vorticity between -7 and 7. Inner-region mesh boundary is shown in gray.

To accommodate the motion of this inner region, the cells in the surrounding outer region are set to re-mesh automatically. The re-meshing is performed every iteration and only if the solver detects that the cell size and quality falls outside the ranges specified to maximise cell quality. Figure 2 shows an example of vorticity contours for the cubic deflection profile; the results are smooth in the near-wake region and exhibit only small numerical noise across the re-meshing boundary.

Solution Parameters

The incompressible 2D Navier–Stokes equations are solved directly using a commercially-available finite-volume pressure-based code. An initial solution was obtained using first-order accuracy for one flapping cycle. From this, the solution was run using second-order accuracy in pressure and momentum and Green-Gauss Node-Based gradient discretisation, for a number of cycles until the solution reached a stable periodic state (i.e. cycle-to-cycle variation in peak-to-peak force components less than 5%). The temporal accuracy was limited to first-order due to the limitations of the software when using dynamic meshing.

Spatial Discretisation

The domain was discretised using a C-type structured mesh around the airfoil and immediately downstream, as shown in Figure 3, transitioning to unstructured cells extending to the far-field boundary. The structured mesh region was intended to capture the boundary layer and the near wake region. For the final mesh the thickness of the structured region around the airfoil was 0.4c, and it extended 1.2c downstream of the trailing edge (still well within the inner region boundary beyond which remeshing occurs). The chordwise cell spacing was of the order of 0.002c, with more cells clustered at the leading and trailing edges of the airfoil.

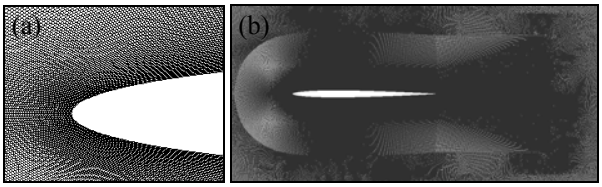

Figure 3. Mesh around NACA0005 airfoil; (a) close-up around leading edge and (b) overall structured region.

Verification and Validation

A grid and time-step independence study was performed on the NACA0005 airfoil mesh, as it was expected that this thinner airfoil would require higher spatial and temporal resolution.

The grid independence was verified by comparing the force histories computed using the mesh described above, with a finer resolution mesh. The finer mesh had a larger structured region (thickness 0.6c and extending 1.6c downstream) and the number of wall-parallel and wall-normal cells was increased by roughly 50%, so that the total mesh size was approximately doubled. The meshes were tested for the case of quadratic chordwise flexure, and for both thrust and power the solution was found to change by no more than 2% of the total range. Therefore, the spatial resolution of the coarser mesh was judged sufficient.

The time-step independence study was performed using the coarser mesh and quadratic flexure. The force prediction was compared for 1000 time-steps per cycle (used in the grid-independence) with 2000 time-steps per cycle. Halving the time-step changed the instantaneous force histories by less than 4% of the range, so 1000 time-steps per cycle was judged sufficient for a temporally resolved simulation.

These time-step and the coarser-mesh settings were applied to a NACA0014 airfoil for validation against Miao & Ho [7]. The

comparison in the drag history is shown in Figure 4 for the quadratic-flexure case; the overall agreement is good. There is a slight difference in the magnitudes and a small phase offset, which could be attributed to uncertainty in the digitisation, or related to Miao & Ho using a compressible simulation (with a free stream mach number of 0.1). The comparisons were similar for the lift and for the zero-flexure case (not shown).

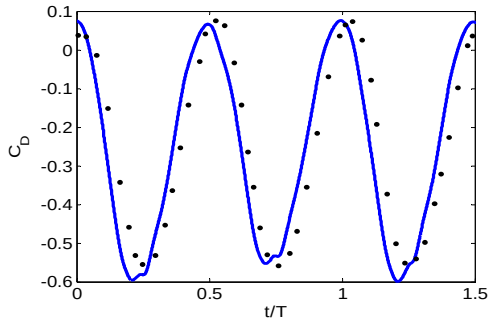

Figure 4. Comparison of drag coefficient calculated for quadratic flexing in current study (heavy line) and Miao & Ho [7] ('•').

Asymmetry in Linear Case

For the linear profile, Figure 5 shows the thrust and input-power time-history. An asymmetry is evident near the points of maximum thrust (i.e. at mid-stroke). This pattern was repeated across four cycles with less than 3% variation and therefore is not attributed to cycle-to-cycle variability. Because the motion and the geometry are symmetric, it is not obvious why there should be an asymmetry in the forces. However asymmetric force production for symmetric flapping wings has been reported in a number of other 2D simulations (e.g. [2],[9]) and experimental studies [9]. Yu, Hu & Wang [9] proposed that when the aerodynamic parameters are within certain ranges, small disturbances in the flow are amplified (for example upstream tunnel conditions in experiments or initial conditions in simulations).

To check the validity of the present results, the grid and time-step independence studies were repeated for the linear flexing profile: the cycle-average thrust and power changed by no more than 1% and the asymmetry remained. For a_0=0.2 the maximum pitch-angle magnitude about the leading edge was 11.3º, and the chord length changed by less than 2% when the shearing-type motion was used, so this deflection profile is similar to a rigid wing pitching about the leading-edge. A simulation was performed with an equivalent rigid wing to rule out possible numerical perturbations introduced by re-gridding; a similar asymmetry was observed, and the average solution changed by no more than 1%.

Results

Instantaneous thrust and power profiles

The thrust and input-power coefficients (based on reference velocity V_∞ and length c) for the flexing profiles and $a_0 = 0.2$ are given in Figure 5. In order of increasing deflection along the wing, the deflection profiles are cubic, quadratic, quadratic-2 and linear. Although the leading and trailing displacements are the same through the cycle, there is a significant difference in the thrust production – as the deflection along the wing increases, the thrust production consistently increases. The power consumption also increases, but not as significantly (not shown).

Because the linear-type flexing profile generates the most thrust for the chosen tip deflection a_0, the effect of changing a_0 for the linear profile was also examined. This parameter study has previously been considered in [7] for the quadratic profile, and the thrust efficiency was found to be maximised for a_0 = 0.3. However due to the force-history asymmetry observed for a_0 = 0.2 in the linear case, only $a_0 \leq 0.2$ are tested here. Increasing a_0 progressively increases the thrust as shown in Figure 6, but unlike the quadratic and cubic deflection profiles the mean power consumption decreases, as will be shown in the next section.

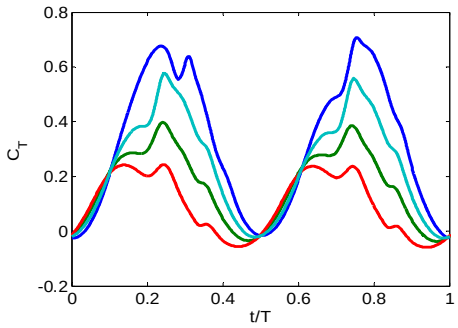

Figure 5. Thrust coefficient over a typical flapping cycle, (a) thrust and (b) input power, for basic flexing profiles: cubic; quadratic; quadratic-2; linear.

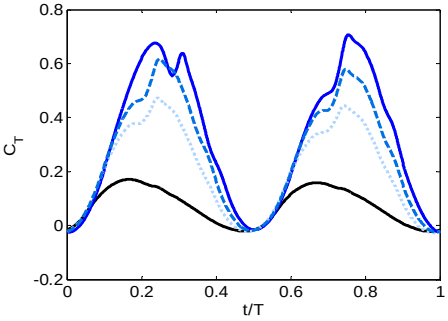

Figure 6. Thrust coefficient over a typical flapping cycle, for linear-type flexing profiles with varying tip deflection magnitude: a_0 = 0.2; a_0 = 0.15; a_0 = 0.1; a_0 = 0 (i.e. no flexing).

Cycle-averaged quantities

The degree of deflection can be quantified by considering the mean deflection amplitude of the profile, as follows

$$\bar{y} = \frac{a_o}{c} \int f(x)dx. \qquad (5)$$

A higher value of $\bar{y}$ corresponds to a greater average inclination of the wing to the oncoming flow. $\bar{y}$ also serves as a measure of the mean wing deflection velocity and acceleration. Because the net force is dominated by the pressure (approximately 99%) and pressure acts normal to the wing, increasing deflection allows a greater proportion of the total force to act in the thrust direction.

The cycle-averaged input power, thrust and efficiency are shown against mean deflection amplitude in Figure 7. For the basic flexing profiles, Figure 7(a) shows a consistent increase in all quantities with mean deflection. The relative variation in power is small compared to the thrust, so efficiency and thrust follow a similar (and approximately linear) trend with mean deflection amplitude. This suggests that the details of the curvature in the wing flexure are relatively insignificant; the thrust performance is largely dependant on the net flexure displacement of the wing. The highest efficiency is obtained with the linear profile, which (as mentioned earlier) is comparable to a rigid wing pitching

about the leading edge. This indicates that for simple flapping kinematics, the best thrust performance may be obtained with a simple wing which is free to pitch passively about the leading edge.

Figure 7(b) illustrates the results for the linear-based deflection profiles with varying tip amplitudes. With increasing mean deflection (now proportional to a_0) the power coefficient decreases, contrary to the trend observed for the basic flexing profiles. However the thrust and the efficiency still increase, indicating that overall a high degree of chordwise flexure is favourable in terms of thrust performance. However it is noted that for $a_0 < 0.2$ the aforementioned asymmetry is not observed, which suggests that for smaller tip deflection magnitudes the force production is more stable. Further simulations would be required to determine if this behaviour extends to 3D.

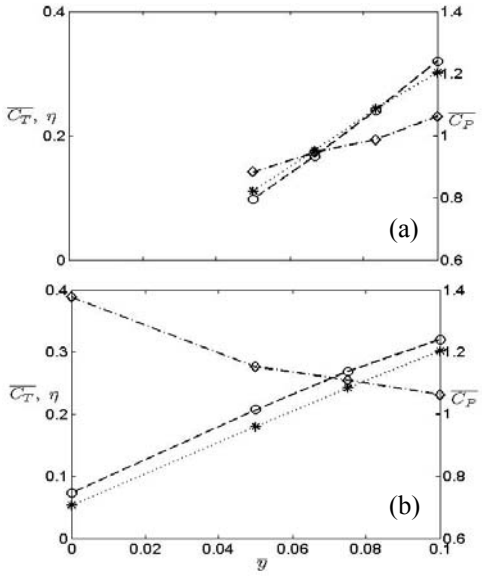

Figure 7. Cycle-averaged performance parameters versus mean deflection amplitude for (a) basic profiles and (b) linear profiles with varying a_0; 'o' thrust coefficient $\overline{C_T}$, '*' efficiency η, and '◊' power coefficient $\overline{C_P}$.

Although in both groups increasing the mean deflection increases the efficiency almost linearly, the results do not all fall on the same trend. For a given tip deflection, a linear-based profile performs better (in terms of thrust and efficiency) than a curved profile**.** Figure 8 shows the instantaneous pressure-coefficient distribution halfway through the downstroke (where the forces are greatest) for the cubic and the linear profile with $a_0 = 0.2$. The force generation is primarily from the upstream side of the wing and is primarily due to the suction peaks that arise as a result of the leading-edge vortex (LEV), as shown in the insert to Figure 8 for linear profile. Although the two profiles have the same $\overline{y}$, the linear profile generates a stronger pressure force. Additionally, over the first third of the wing the linear profile flexes more than the cubic profile, so a greater proportion of the LEV-based pressure force will act in the thrust direction. The result is that the linear flexure profiles are able to generate thrust more efficiently.

Conclusion

The aerodynamic performance of 2D airfoils undergoing flapping and various flexing profiles were considered. For a given trailing edge tip deflection magnitude, the main factor influencing the thrust efficiency for the chosen kinematics is the mean deflection amplitude of the flexing wing. Within the range of parameters considered, the maximum thrust and thrust-to-power efficiency was obtained for a linear wing flexing with a tip deflection of 20% chord (the highest tested).

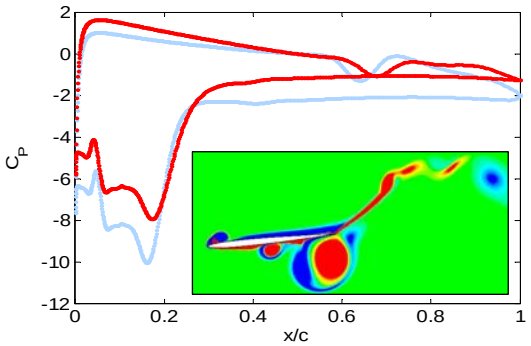

Figure 8. Instantaneous pressure distribution at t/T = 0.25; — cubic profile, — linear profile with a_0 = 0.1. Shown in the insert are contours of vorticity between -7 and 7 for the linear deflection profile with a_0 = 0.1 at t/T = 0.25.

References

[1] Beng, T.W., *Analysis of Non-Symmetric Flapping Airfoils and Their Configurations***,** PhD thesis, National University of Singapore, 2009.

[2] Bos, F.M., Lentink, D., van Oudheusden, B.W., & Bijl, H., Influence of Wing Kinematics on Aerodynamic Performance in Hovering Insect Flight., *J. Fluid Mech.*, **594**, 2008, 341–368.

[3] Ellington, C.P., The Novel Aerodynamics of Insect Flight: Applications to Micro-Air-Vehicles, *J. Exp. Biology*, **202**, 1999, 3439–3448.

[4] Heathcote, S., Martin, D., & Gursul, I., Flexible Flapping Airfoil Propulsion at Zero Freestream Velocity, *AIAA J.*, **42**(11), 2004, 2196–2204.

[5] Heathcote, S., Wang, Z., & Gursul, I., Effect of Spanwise Flexibility on Flapping Wing Propulsion, *J. Fluids & Structures*, **24**, 2008, 183–199.

[6] Lentink, D. & Gerritsma, M.Influence of Airfoil Shape on Performace in Insect Flight, 33rd AIAA Fluid Dynamics Conf., 23–26 June 2003, Orlando, FL.

[7] Miao, J-M., & Ho, M-H., Effect of Flexure on Aerodynamic Propulsive Efficiency of Flapping Flexible Airfoil, *J. Fluids & Structures*, **22**, 2006, 401–419.

[8] Tang, J., Viieru, D., & Shyy, W., A Study of Aerodynamics of Low Reynolds Number Flexible Airfoils, *37th AIAA Fluid Dynamics Conf.*, 25–28 June 2007, Miami, FL.

[9] Yu, M. L., Hu, H., & Wang, Z.J., Experimental and Numerical Investigations on the Asymmetric Wake Vortex Structures Around an Oscillating Airfoil, *50th AIAA Aerospace Sci. Meeting*, 09–12 January 2012, Nashville, Tennessee.

[10] Yuan, W., Lee, R., Hoogkamp, E., & Khalid, M., Numerical and Experimental Simulations of Flapping Wings, *Int. J. Micro Air Vehicles*, **2(3)**, 2010, 181–208.

[11] Zhao.,L., Deng, X., & Sane, S.P., Modulation of Leading Edge Vorticity and Aerodynamic Forces in Flexible Flapping Wings, *Bioinspiration & Biomimetics*, **6**, 2001.